Biophysical Journal

Supporting Material

The semiquinone-iron complex of Photosystem II: structural insights from ESR and theoretical simulation. Evidence that the native ligand to the non-heme iron is carbonate.

Nicholas James Cox, Lu Jin, Adrian Jaszewski, Paul J Smith, Elmars Krausz, William Alfred Rutherford, and Ron J. Pace

SUPPORTING INFORMATION

S1: Simple Picture - Iron (Fe^{2+}), quinone energy levels

The non-heme iron center of the BRC is high spin d^6 (Fe^{2+}, S = 2) (*1*). The number of distinct electronic configurations (210) that the system can adopt is prohibitively large, posing a daunting theoretical exercise. The problem can be significantly simplified by assuming the ground state is a quintet (2S+1), energetically well removed from higher electronic states. (e.g. see (*1*) for a justification of this).

The energy level splittings within the ground state orbital manifold can be well described using the spin Hamiltonian formalism with quadratic zero-field parameters; the axial (D) and rhombic (E) terms. For the BRC, the D and E terms were estimated as 7.6 and 1.9 K respectively, using bulk magnetization measurements (*2*). This yields a ground to first excited state energy difference of ~3 K, and a ground to second excited state energy difference of ~12 K.

When weakly coupled to the Q_A^- center, each singlet sublevel of the iron manifold becomes a Kramer's doublet, which splits in the presence of a magnetic field. Allowed ESR transitions occur within these doublets (i.e. 5 observable spin-allowed transitions, all contributing to the observed ESR semiquinone-iron signal, Fig. s1). In these studies the microwave frequency (9 GHz, 0.43 K) is too low to induce transitions between doublet states. Over the temperature range (5-20 K) used here the ESR signal is dominated by the two lowest doublet transitions.

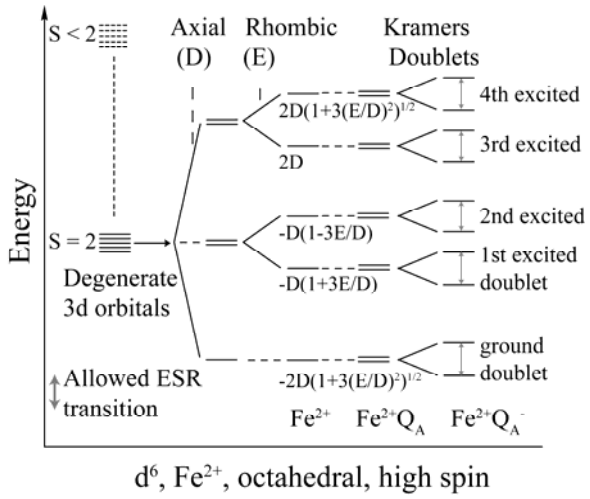

Figure s1: Pictorial representation of the energy-levels of the semiquinone-iron system

S2: Decomposition of the semi-quinone iron signal: effective g_X, g_Y, g_Z positions

It is instructive to examine how the iron-semi-quinone signals arise. The ESR spectrum of the isolated semi-quinone radical is near isotropic at g~2. Addition of the Fe^{2+} center introduces a magnetization (*effective* internal magnetic field) along the molecular y axis. The electron spin on the quinone then sees two distinctly different environments. When viewed along either x or z, the system appears unperturbed (transition at g~2). Along y, the semi-quinone sees an *effective* magnetic field from the external field and the iron induced internal

field. For the ground state, as the magnetization of the Fe^{2+} sublevel is negative, the effective field is decreased, shifting the ESR transition to higher external field. Similarly, for the 1st excited state the total effective field is raised, shifting the ESR transition to lower external field. A pictorial representation of the powder pattern spectra corresponding to the ground and 1st excited state transitions is shown in Fig. s2 A. 2nd order effects lead to a breaking of the x, z degeneracy as seen in the real systems as indicated in Fig. s2 B, C. The maxima of the ground and first excited state appear symmetrically about g~1.8 for the BRC signal. Their sum yields the relatively sharp prominent feature of the ESR signal. The absorbance spectrum of the g~1.9 signal is very similar. Compared to the g~1.84 signal, the maximum for each doublet (nominally the average of the effective g_X and g_Z positions) separate; the ground state maximum shifts to high field, the first excited state maximum to low field. This decomposition is consistent with the temperature dependence of the signal - the high field edge is lost as the observation temperature increases.

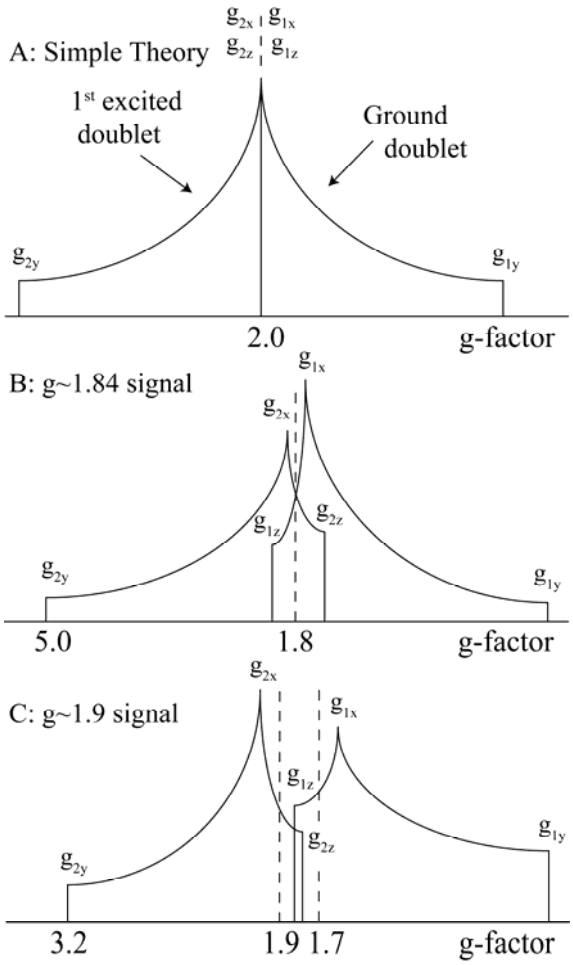

Figure s2: Decomposition of the semiquinone-iron signal into its two lowest ESR transitions. Marked g positions (g_X, g_Y, g_Z) show the effective g tensor values as calculated by third order perturbation theory (see text). Panel A: simple theory; panel B: g~1.84 signal; panel C: g~1.9 signal.

S3: Perturbation analysis of the g~1.9 semi-quinone iron signal; the uniqueness of the simulation

The Spin Hamiltonian (Eq. 1) has 8 independent variables: g_X, g_Y, g_Z, J_X, J_Y, J_Z, D and E. In the simulation of the g~1.84 signal in BRC (*1*), the iron g tensor and fine structure parameters had been determined by bulk magnetization measurements prior to the simulation (*2*). This limited the number of independent variables in this simulation to three. The same experimental data were not available for this work; no independent estimate of the fine structure or g tensor parameters has been made for PS II. As a consequence, an effort was made to examine the uniqueness of the system's optimized parameter set (see Fig. 3, Table 1) using analytical relationships derived from perturbation theory. We note that the structural equivalence of PS II and BRC (*3-6*) strongly suggests that these parameters will be very similar. Hence we limited this investigation to the parameter set where the exchange and zero-field tensor components were comparable to estimates for the BRC i.e. 1-20 K.

Butler et al (*1*) used 3rd order perturbation theory to derive expressions (in terms of the exchange coupling, zero-field parameters etc) for the effective g-value positions as shown in Fig. 5 B. The effective Hamiltonian for each doublet of the system takes the form (*1*):

$$H_i = E_i' + \beta H \cdot g_i \cdot S_Q \qquad \text{(A1)}$$

Here E_i describes all terms that are independent of the operator S_Q, while g_i is the diagonal effective g tensor (with principle values defining the turning points of the absorbance spectrum shown above). The solution to this effective Hamiltonian along the three principle axes is provided below.

	g_0	$\delta g_i^{(1)}$	$\delta g_i^{(2a)}$	$\delta g_i^{(2b)}$
g_{1x}	g_Q	$\frac{2\cdot Q^2}{E_{31}} J_x g_{Fe_x}$	$-\frac{g_Q}{2}\left[\frac{J_y P^2}{E_{21}^2}+\frac{J_z (P+Q)^2}{E_{41}^2}\right]$	$g_{Fe_x} J_y J_z \left[\frac{P(P+Q)}{E_{21}E_{41}}-\frac{Q(P+Q)}{E_{31}E_{41}}+\frac{PQ}{E_{21}E_{31}}\right]$
g_{1y}	g_Q	$\frac{2\cdot P^2}{E_{21}} J_y g_{Fe_y}$	$-\frac{g_Q}{2}\left[\frac{J_x Q^2}{E_{31}^2}+\frac{J_z (P+Q)^2}{E_{41}^2}\right]$	$g_{Fe_y} J_x J_z \left[\frac{Q(P+Q)}{E_{21}E_{41}}+\frac{P(P+Q)}{E_{21}E_{31}}-\frac{PQ}{E_{21}E_{41}}\right]$
g_{1z}	g_Q	$\frac{2\cdot (P+Q)^2}{E_{51}} J_z g_{Fe_z}$	$-\frac{g_Q}{2}\left[\frac{J_x Q^2}{E_{31}^2}+\frac{J_y P^2}{E_{21}^2}\right]$	$g_{Fe_z} J_y J_x \left[-\frac{P(P+Q)}{E_{21}E_{41}}-\frac{Q(P+Q)}{E_{31}E_{41}}-\frac{PQ}{E_{21}E_{31}}\right]$
g_{2x}	g_Q	$\frac{2}{E_{42}} J_x g_{Fe_x}$	$-\frac{g_Q}{2}\left[\frac{J_y^2 P^2}{E_{31}^2}+\frac{J_y^2 S^2}{E_{51}^2}+\frac{J_z^2}{E_{32}^2}\right]$	$g_{Fe_x} J_y J_z \left[-\frac{RS}{E_{32}E_{52}}+\frac{PQ}{E_{21}E_{32}}+\frac{P(P+Q)}{E_{21}E_{42}}+\frac{1}{E_{32}E_{41}}-\frac{(R+S)S}{E_{42}E_{52}}\right]$
g_{2y}	g_Q	$\left[-\frac{2\cdot P^2}{E_{21}}+\frac{2\cdot S^2}{E_{52}}\right] J_y g_{Fe_y}$	$-\frac{g_Q}{2}\left[\frac{J_x{}^2}{E_{41}^2}+\frac{J_y{}^2}{E_{32}^2}\right]$	$g_{Fe_y} J_x J_z \left[-\frac{1}{E_{32}E_{42}}+\frac{RS}{E_{32}E_{52}}-\frac{PQ}{E_{21}E_{32}}+\frac{P(P+Q)}{E_{21}E_{42}}-\frac{(R+S)S}{E_{42}E_{52}}\right]$
g_{2z}	g_Q	$\frac{2}{E_{31}} J_z g_{Fe_z}$	$-\frac{g_Q}{2}\left[\frac{J_y^2 P^2}{E_{31}^2}+\frac{J_y^2 S^2}{E_{51}^2}+\frac{J_x^2}{E_{52}^2}\right]$	$g_{Fe_z} J_y J_x \left[-\frac{P(P+Q)}{E_{21}E_{42}}+\frac{(R+S)S}{E_{42}E_{52}}+\frac{RS}{E_{32}E_{52}}-\frac{PQ}{E_{21}E_{32}}+\frac{1}{E_{32}E_{42}}\right]$

(A2) (Taken from Butler et al (*1*))

All tensors taken to be diagonal, subscripts refer to the xx, yy and zz components etc
g_i is the effective g-tensor for the i^{th} doublet
$g_i^{(0)}$ is the zero order result for the g-value
$\delta g_i^{(x)}$ is the x^{th} order correction to the g-value
J is the exchange coupling tensor

E_{ij} is the zero field energy difference between doublets i and j

$$P = \frac{\sqrt{1+3(E/D)^2}-1+3(E/D)}{\left[\left(\sqrt{1+3(E/D)^2}-1\right)^2+3(E/D)^2\right]^{1/2}}$$

$$Q = \frac{\sqrt{1+3(E/D)^2}-1-3(E/D)}{\left[\left(\sqrt{1+3(E/D)^2}-1\right)^2+3(E/D)^2\right]^{1/2}}$$

$$R = \frac{\sqrt{1+3(E/D)^2}+1+3(E/D)}{\left[\left(\sqrt{1+3(E/D)^2}+1\right)^2+3(E/D)^2\right]^{1/2}}$$

$$S = \frac{\sqrt{1+3(E/D)^2}+1-3(E/D)}{\left[\left(\sqrt{1+3(E/D)^2}+1\right)^2+3(E/D)^2\right]^{1/2}} \qquad \text{(A3)}$$

As discussed above, the mean position of the g_X and g_Z turning points in either the ground or first excited state for the g~1.84 signal are at g = 1.8 (see Fig. s2). That is to say:

$$\begin{aligned} \tfrac{1}{2}(g_{1x}+g_{1z}) &= 1.8 \\ \tfrac{1}{2}(g_{2x}+g_{2z}) &= 1.8 \end{aligned} \qquad \text{(A4)}$$

For the g~1.9 signal analogous equations can be generated. Here though the mean positions of g_X and g_Z differs for the ground and first excited state.

$$\begin{aligned} \tfrac{1}{2}(g_{1x}+g_{1z}) &= 1.69 \quad \text{ground} \\ \tfrac{1}{2}(g_{2x}+g_{2z}) &= 1.89 \quad \text{1st excited} \end{aligned} \qquad \text{(A5)}$$

Hence for either signal we can impose two constraints. As the parameter space for the g~1.84 signal is three (the J tensor principal values), this system of equations has one degree of freedom. By comparison, the g~1.9 signal has eight free parameters (g_{Fe} tensor, J tensor, fine structure tensor) and consequently a total of six degrees of freedom.
To further reduce the free parameter set for the g~1.9 signal simulation, the g tensor of the iron was assumed to be the same as for the g~1.84 signal, as it was observed that varying the components of the iron g tensor had little effect on the overall fit. This assumption reduced the degrees of freedom for the g ~1.9 system to three.

Fig. s3 graphically demonstrates the solutions to Eqs. A4 and A5. Panel A shows the original solutions of Bulter et al. (*1*) (g~1.84 signal) for Eq. 3 with the simulation fit values for the J components superimposed. It can be seen that the numerical solution is near the point of maximum isotropy for J. In this solution region J_Z is always larger (in magnitude) than J_X. Panel B shows the solutions of Eq. 4 (g~1.9 signal), assuming the zero-field

splitting parameters of Bulter et al. (*1*) This now requires J_X to be larger (in magnitude) than J_Z in the corresponding solution region. Importantly however no good fit to the experimental spectrum could be obtained using these fine structure values (D = 7.6, E/D = 0.25). Panel C shows the solutions to Eq. A5 using the D and E values found necessary to fit the experimental spectra at both 5 and 15 K. Here as when D = 7.6 K, the magnitude ordering of J_X and J_Z was opposite to that in panel A. It was shown that this ordering inversion occurs for all plausible values of D (1-20 K). Thus the solution fit parameters as determined for the g~1.9 signal are robust by this analysis. Even though in exchange-coupled systems anisotropy is typically modest (*1; 7*), as indeed is seen for the g~1.84 signal, the exchange anisotropy occurring in the g~1.9 species appears to be genuinely large. Interestingly, the isotropic component of the coupling is virtually the same in both the g~1.84 and g~1.9 forms (Table 1).

Although the above analysis assumes that the exchange and zero field tensors are co-linear and the precise quantitative conclusions are contingent on this, *qualitatively,* a significant change in the relative orientation of the exchange tensor between the two signal types seems inescapable.

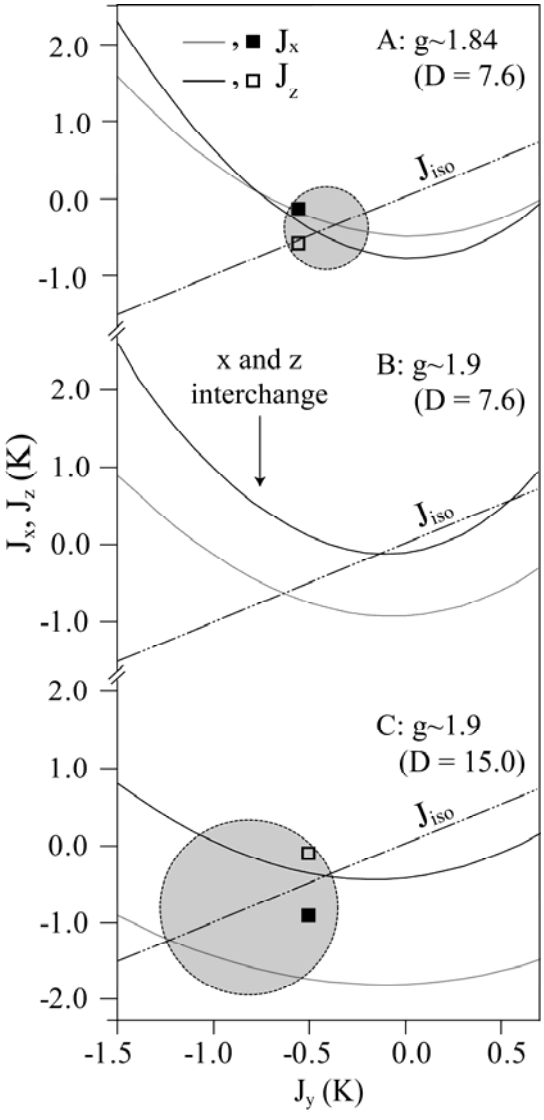

Figure s3: Estimates of the exchange coupling tensor for the semiquinone-iron signal along the three principle axes (see text). Panel A: J_X and J_Z values as a function of J_Y (from Eq. 3) of the g~1.84 signal (as per Butler et al. 1984). Panel B: J_X and J_Z values as a function of J_Y (from Eq. A4) of the g~1.9 signal, using zero-field parameters as per Bulter et al. (D = 7.6 K, E/D = 0.25). Panel C: J_X and J_Z values as a function of J_Y (from Eq. A5) of the g~1.9 signal, using the fitted zero-field parameters determined here (D = 15.0 K, E/D = 0.25). Filled and unfilled squares represent the simulation fit values of J_X and J_Z respectively. The circles represent the minimum radius regions centered on the purely isotropic solution points, which include the simulation J values.

S4: Powder Pattern

The paramagnetic centers of a frozen ESR sample take all possible orientations (relative to the field axis), often referred to as a powder pattern. As the semi-quinone iron system is anisotropic, to correctly simulate the ESR spectrum all unique orientations have to be included.

The simulation code allows for this effect by using combination of Euler rotations (α and β) see diagram. This system only requires two Euler rotations to define all unique orientations as rotation about the field axis does not alter the eigenvalues of the system.

A generalized powder pattern code was adopted (shown below). The typical number of β angles used (n) ranged from 20-100. Dummy variables x and y were used to uniformly sample the hemisphere. For a given x (β) angle 1 to p(x+1) y (α) angles were sampled (with the entries of p(x) as defined below). Note: for x =0 (β=0), α was also set to zero.

For x = 0 to n-1
For y = 1 to p(x+1)

$$p(x+1) = \left(\frac{360}{90/(n-1/2)} \right) \cdot \sin\left(\left(90/(n-1/2) \right) \cdot x \right)$$

$$\beta = x \cdot \left(\frac{90}{n-1/2} \right)$$

$$\alpha = \left(y - 1/2 \right) \cdot \left(\frac{360}{p(x+1)} \right)$$

Eq. A6

α and β angles define the rotation matrix as below (*8*):

$$R = \begin{bmatrix} \cos(\alpha)\cdot\cos(\beta) & \sin(\alpha)\cdot\cos(\beta) & -\cos(\beta) \\ \sin(\alpha) & \cos(\alpha) & 0 \\ \cos(\beta) & \sin(\alpha)\cdot\sin(\beta) & \cos(\beta) \end{bmatrix}$$

The unitary transformation $T^* = R \cdot T \cdot R'$ was applied to the tensors (*8*):

$$D^{*} = R \cdot D \cdot R'$$

$$g_{Fe}{}^{*} = R \cdot g_{Fe} \cdot R'$$

$$J^{*} = R \cdot J \cdot R' \qquad \text{Eq. A7}$$

S5: Transition Intensities

The intensity of transition between the i^{th} and j^{th} state is given the equation below (*9*):

$$I \propto \left| \langle i | \beta H_1 \cdot g_{Fe} \cdot S_{Fe} + g_Q \beta H_1 \cdot S_Q | j \rangle \right|^2 \qquad \text{Eq. A8}$$

Where the oscillating H_1 field lies in the x-y plane (perpendicular to H). All of its possible orientations must be included to correctly estimate transition intensities. This is achieved by averaging over the third Euler angle (γ) (*8*). H_1 can be expressed as:

$$H_1 = \begin{bmatrix} \cos(\gamma) \\ \sin(\gamma) \\ 0 \end{bmatrix}$$

hence

$$I \propto \left| \langle i | \frac{H^2 \beta^2}{2} \left(\cos(\gamma) \cdot \alpha + \sin(\gamma) \cdot \beta \right) | j \rangle \right|^2$$

where

$$\alpha = \left(g_{xx} - i g_{xy} \right) \cdot S^{+} + \left(g_{xx} + i g_{xy} \right) \cdot S^{-} + 2 g_{xz} S_z$$

$$\beta = \left(g_{yx} - i g_{yy} \right) \cdot S^{+} + \left(g_{yx} + i g_{yy} \right) \cdot S^{-} + 2 g_{yz} S_z$$

Integrating with respect to γ yields:

$$\int_0^{2\pi} (\alpha \cdot \cos(\gamma) + \beta \cdot \sin(\gamma))^2 \, d\gamma$$

$$= \int_0^{2\pi} \frac{\alpha^2}{2} \cdot (1 + \cos(2\gamma)) + \frac{\beta^2}{2} \cdot (1 - \cos(2\gamma)) + \alpha\beta \sin(2\gamma) d\gamma$$

$$= \left| \frac{\alpha^2}{2} (\gamma + \tfrac{1}{2} \sin(2\gamma)) + \frac{\beta^2}{2} (\gamma - \tfrac{1}{2} \sin(2\gamma)) - \frac{\alpha\beta}{2} \cos(2\gamma) \right|_0^{2\pi}$$

$$= \pi(\alpha^2 + \beta^2)$$

The transition intensity can therefore be expressed as:

$$I \propto \left| \langle i | \frac{\pi H^2 \beta^2 \left(\alpha^2 + \beta^2 \right)}{2} | j \rangle \right|^2 \qquad \text{Eq. A9}$$

S6: Frequency to field correction

An additional correction, first identified by Aasa and Vanngard (*10*), was required to accurately simulate the transition intensity. This takes into account that equation A5, the transition intensity, is *frequency* rather than field dependent.

The integrated intensity of a EPR signal (of shape defined by S(H)) in frequency space is given by the equation below:

$$\int I \cdot S(H)dH = \int I \cdot f(\upsilon) \cdot \frac{dH}{d\upsilon} d\upsilon \qquad \text{Eq. A10}$$

If we assume the line-shape function S(H) is Gaussian:

$$S(H) = A \cdot e^{-\left(\frac{H-H_0}{w}\right)^2}$$

then

$$\int S(H)dH = A \cdot w \cdot \sqrt{\pi} = \int f(\upsilon) \cdot \frac{dH}{d\upsilon} d\upsilon$$

Assuming dH/dν is constant over the Gaussian, the magnitude of the Gaussian in field space is simply proportional to the change in magnetization (dH/dν).

$$A \propto \frac{dH}{d\nu}$$

So the line-shape of a particular point in the powder pattern (α/ β angle combinations) takes the form:

$$S(\alpha,\beta) = \frac{1}{\left(A \cdot w \cdot \frac{dH(\alpha,\beta)}{d\upsilon}\right)} e^{-\left(\frac{H(\alpha,\beta)-H}{w}\right)^2} \qquad \text{Eq. A11}$$

S7: Full Matrix Representation of the Spin Hamiltonian

The matrix representation of equation 1 is shown below:

$$H = S_{Fe} \cdot D \cdot S_{Fe} + \beta H \cdot g_{Fe} \cdot S + g_Q \beta H \cdot S - S_{Fe} \cdot J \cdot S_Q$$

$$H = \begin{bmatrix}
F+Q+Z+C & C & F+Z+C & C & Z \\
C & F+Q+Z+C & C & F+Z+C & 0 \\
F+Z+C & C & F+Q+Z+C & C & F+Z+C \\
C & F+Z+C & C & F+Q+Z+C & C \\
Z & 0 & F+Z+C & C & F+Q+Z+C \\
0 & Z & C & F+Z+C & 0 \\
0 & 0 & Z & 0 & F+Z+C \\
0 & 0 & 0 & Z & C \\
0 & 0 & 0 & 0 & Z \\
0 & 0 & 0 & 0 & 0
\end{bmatrix}$$

$$\begin{bmatrix}
0 & 0 & 0 & 0 & 0 \\
Z & 0 & 0 & 0 & 0 \\
C & Z & 0 & 0 & 0 \\
F+Z+C & 0 & Z & 0 & 0 \\
0 & F+Z+C & C & Z & 0 \\
F+Q+Z+C & C & F+Z+C & 0 & Z \\
C & F+Q+Z+C & C & F+Z+C & C \\
F+Z+C & C & F+Q+Z+C & C & F+Z+C \\
0 & F+Z+C & C & F+Q+Z+C & C \\
Z & C & F+Z+C & C & F+Q+Z+C
\end{bmatrix}$$

Where:
F = Zeeman term for the iron (Fe^{2+}) center

$$H_Z = \frac{\hbar \beta H_Z}{2}\left[S_{Fe}{}^{+}(g_{zx} - ig_{zy}) + S_{Fe}{}^{-}(g_{zx} + ig_{zy})\right] - 2\hbar g_{zz}\beta H_Z S_{FeZ}$$

Q = Zeeman term for the semi-quinone

$$H_Q = \hbar g_Q \beta H_Z S_Z$$

Z = zero field splitting

$$H_Z = \frac{1}{4}(S_{Fe}{}^{+2} + S_{Fe}{}^{-2})(D_{xx} - D_{yy}) + \frac{1}{4}(S_{Fe}{}^{+}S_{Fe}{}^{-} + S_{Fe}{}^{-}S_{Fe}{}^{+})(D_{xx} - D_{yy})$$
$$+ \frac{1}{2i}(S_{Fe}{}^{+2} - S_{Fe}{}^{-2})D_{xy} + \frac{1}{2}[(S_{Fe}{}^{+} + S_{Fe}{}^{-})S_{FeZ} + S_{FeZ}(S_{Fe}{}^{+} + S_{Fe}{}^{-})]D_{xz}$$
$$+ \frac{1}{2i}[(S_{Fe}{}^{+} - S_{Fe}{}^{-})S_{FeZ} + S_{FeZ}(S_{Fe}{}^{+} - S_{Fe}{}^{-})]D_{yz} + S_{FeZ}{}^{2}D_{zz}$$

C = Exchange term

$$H_C = \frac{1}{4}(S_{Fe}{}^{+}S_Q{}^{+} + S_{Fe}{}^{-}S_Q{}^{-})(J_{xx} - J_{yy}) + \frac{1}{4}(S_{Fe}{}^{+}S_Q{}^{-} + S_{Fe}{}^{-}S_Q{}^{+})(J_{xx} + J_{yy}) +$$
$$+ \frac{1}{2i}(S_{Fe}{}^{+}S_Q{}^{+} + S_{Fe}{}^{-}S_Q{}^{-})J_{xy} + \frac{1}{2}[(S_{Fe}{}^{+} + S_{Fe}{}^{-})S_{QZ} + S_{FeZ}(S_Q{}^{+} + S_Q{}^{-})]J_{xz}$$
$$+ \frac{1}{2i}[(S_{Fe}{}^{+} - S_{Fe}{}^{-})S_{QZ} + S_{FeZ}(S_Q{}^{+} - S_Q{}^{-})]J_{yz} + S_{FeZ}S_{QZ}J_{zz}$$

S8: Simulation Code

```
stacksize(10000000);

abc=[0.9;.5;0.1;240;15;.27;11000];

function y=QA_fun(abc,m);

// intial parameters
```

```
f=9.436557e9;
B=0.92731e-20;
P=2*%pi*1.05443e-27;
PP=1.05443e-27*1.05443e-27;
kb=1.38044e-16;

// g tensor parameters

gx=2.16;
gy=2.27;
gz=2.04;
gq=2;

// Exchange Interaction

Jx=abc(1);
Jy=abc(2);
Jz=abc(3);

// widths

wx=[abc(4);abc(4);abc(4);abc(4);abc(4)];
wy=[abc(4);abc(4);abc(4);abc(4);abc(4)];
wz=[abc(4);abc(4);abc(4);abc(4);abc(4)];


// Resolution

ss=100;
hadj=30;   // resolution of field
hadj1=30;   //field ranges we need
nnn=30;   // number of beta angles (for powder pattern)
HS=500;     // start of field
RES=80;
HF=HS+RES*ss;
HG=450;
mmm=5;

// Temperature (at which the spectrum was taken)

temp=5;
temp1=15;
D=abc(5);
E=abc(6)*D;

// Crystal Field Parameters

Dx=-1/3*(D-3*E);
```

```
Dy=-1/3*(D+3*E);
Dz=2/3*D;

// Calculation Code

K=[gx 0 0;
   0 gy 0;
   0  0 gz];

J1=2.0837e10*[Jx 0  0;
              0  Jy 0;
              0  0  Jz];

D1=2.0837e10*[Dx 0   0;
              0  Dy  0;
              0  0  Dz];

I=ones(ss,1);
I2=ones(10,1);
h=eye(10,10);
u=zeros(10,1);
T=zeros(ss,3);
Q=zeros(ss,3);
U1=ones(10,10);
U2=tril(U1);
N=[2;6^0.5;6^0.5;2];

// Powder Pattern

for nn=1:nnn;

nnx=90/(nnn-0.5);

n(nn,1)=round((90/nnx)*sin((%pi/180)*nnx*(nn-1)));
n(1,1)=1;

end

// Field Axis

for s=1:ss;

G(s,1)=HS+(s-1)*RES;

end

// Hamiltonian

for x=0:(nnn-1);
for y=1:n(x+1,1);
```

```
if x<1;
b=0;
a=0;
else
b=x*(90/(nnn-0.5))*(%pi/180);
a=(90/n(x+1,1))*(y-0.5)*(%pi/180);
end


J=[cos(a)*cos(b)       sin(a)*cos(b)          -sin(b);
   -sin(a)             cos(a)                 0  ;
   cos(a)*sin(b)       sin(a)*sin(b)          cos(b)];

gi=((gx*J(3,1))^2+(gy*J(3,2))^2+(gz*J(3,3))^2)^0.5;

for hi=0:hadj1;

H=HS+HG/2+hi*HG;

hhh(hi+1,1)=H;

M=zeros(10,10);
M=sparse(M);
R=zeros(10,10);
R=sparse(R);
S=zeros(10,10);
S=sparse(S);
U=zeros(10,10);
F=zeros(10,10);
totbolt=0;
totbolt1=0;

H0=(P*f)/(gi*B);

K11=J*K*J';
J11=(P/(B))*J*J1*J';
D11=(P/(B))*J*D1*J';

for i=1:5;
j=1+2*(i-1):2+2*(i-1);
R(j,j)=K11(1,3)*(-2+(i-1));
S(j,j)=K11(2,3)*(-2+(i-1));
end

for w=1:4;
for i=1+2*(w-1):2+2*(w-1);
R((2+i),i)=N(w,1)*(K11(1,1)-%i*K11(1,2))/2;
R(i,(2+i))=N(w,1)*(K11(1,1)+%i*K11(1,2))/2;
S((2+i),i)=N(w,1)*(K11(2,1)-%i*K11(2,2))/2;
```

```
S(i,(2+i))=N(w,1)*(K11(2,1)+%i*K11(2,2))/2;
end
end

for i=1:5;
j=1+2*(i-1);
R(j+1,j)=gq/2;
R(j,j+1)=gq/2;
S(j+1,j)=gq/(2*%i);
S(j,j+1)=-gq/(2*%i);
end

//electronic zeeman iron

  //off diagonal (x and y)

for w=1:4;
for i=1+2*(w-1):2+2*(w-1);
M((2+i),i)=H/(2)*N(w,1)*(K11(3,1)+%i*K11(3,2));
M(i,(2+i))=H/(2)*N(w,1)*(K11(3,1)-%i*K11(3,2));
end
end

  //diagonal (z)

for i=1:5;
for j=1+2*(i-1):2+2*(i-1);
M(j,j)=H*K11(3,3)*(-2+(i-1));
end
end

//electronic zeeman quinone

  //diagonal (z)

for i=1:5;
j=1+2*(i-1);
M(j,j)=M(j,j)-gq*H/(2);
M(j+1,j+1)=M(j+1,j+1)+gq*H/(2);
end

// Crystal Field

  //diagonal (z)

for i=1:5;
for j=1+2*(i-1):2+2*(i-1);
M(j,j)=M(j,j)+1/2*D11(3,3)*(3*(-2+(i-1))^2-6);
end
end
```

```
  //zero field coupling 1

for i=1:3;
for j=1+2*(i-1):2+2*(i-1);
M(j+4,j)=M(j+4,j)+1/4*N(i+1,1)*N(i,1)*(D11(1,1)-D11(2,2));
M(j,j+4)=M(j,j+4)+1/4*N(i+1,1)*N(i,1)*(D11(1,1)-D11(2,2));
end
end

  //zero field coupling 2

for i=1:3;
for j=1+2*(i-1):2+2*(i-1);
M(j+4,j)=M(j+4,j)-1/2*%i*N(i+1,1)*N(i,1)*(D11(1,2));
M(j,j+4)=M(j,j+4)+1/2*%i*N(i+1,1)*N(i,1)*(D11(1,2));
end
end

  //zero field coupling 4

for i=1:4;
for j=1+2*(i-1):2+2*(i-1);
M(j+2,j)=M(j+2,j)+1/2*N(i,1)*(-2+(i-1))*D11(1,3);
M(j,j+2)=M(j,j+2)+1/2*N(i,1)*(-2+(i-1))*D11(1,3);
M(j+2,j)=M(j+2,j)+1/2*N(i,1)*(-1+(i-1))*D11(1,3);
M(j,j+2)=M(j,j+2)+1/2*N(i,1)*(-1+(i-1))*D11(1,3);
end
end

   //zero field coupling 5

for i=1:4;
for j=1+2*(i-1):2+2*(i-1);
M(j+2,j)=M(j+2,j)-1/2*%i*N(i,1)*(-2+(i-1))*D11(2,3);
M(j,j+2)=M(j,j+2)+1/2*%i*N(i,1)*(-2+(i-1))*D11(2,3);
M(j+2,j)=M(j+2,j)-1/2*%i*N(i,1)*(-1+(i-1))*D11(2,3);
M(j,j+2)=M(j,j+2)+1/2*%i*N(i,1)*(-1+(i-1))*D11(2,3);
end
end

// exchange coupling - iron/ quinone (J1)

  //diagonal (z)

for i=1:5;
j=1+2*(i-1);
M(j,j)=M(j,j)-1/2*J11(3,3)*(-2+(i-1));
M(j+1,j+1)=M(j+1,j+1)+1/2*J11(3,3)*(-2+(i-1));
end
```

```
  //ansiotropic coupling 1

for i=1:4;
j=1+2*(i-1);
M(j+3,j)=M(j+3,j)+1/4*N(i,1)*(J11(1,1)-J11(2,2));
M(j,j+3)=M(j,j+3)+1/4*N(i,1)*(J11(1,1)-J11(2,2));
end

  //anisotropic coupling 2

for i=1:4;
j=2+2*(i-1);
M(j+1,j)=M(j+1,j)+1/4*N(i,1)*(J11(1,1)+J11(2,2));
M(j,j+1)=M(j,j+1)+1/4*N(i,1)*(J11(1,1)+J11(2,2));
end

  //anisotropic coupling 3

for i=1:4;
j=1+2*(i-1);
M(j+3,j)=M(j+3,j)-%i*N(i,1)*1/2*J11(1,2);
M(j,j+3)=M(j,j+3)+%i*N(i,1)*1/2*J11(1,2);
end

  //anisotropic coupling 4

for i=1:4;
j=1+2*(i-1);
M(j+2,j)=M(j+2,j)-1/4*N(i,1)*(J11(1,3)-%i*J11(2,3));
M(j,j+2)=M(j,j+2)-1/4*N(i,1)*(J11(1,3)+%i*J11(2,3));
M(j+3,j+1)=M(j+3,j+1)+1/4*N(i,1)*(J11(1,3)-%i*J11(2,3));
M(j+1,j+3)=M(j+1,j+3)+1/4*N(i,1)*(J11(1,3)+%i*J11(2,3));
end

   //anisotropic coupling 5

for i=1:5;
j=1+2*(i-1);
M(j+1,j)=M(j+1,j)+1/2*(-2+(i-1))*(J11(1,3)-%i*J11(2,3));
M(j,j+1)=M(j,j+1)+1/2*(-2+(i-1))*(J11(1,3)+%i*J11(2,3));
end

//diagonalisation/ eiganvalues/ intensity calculation

M=full(M);

Z=bdiag(M)*I2;

[W,Z111]=spec(M);
```

```
Z1=gsort(real(Z),'r','i');
Z2=diag(Z1);

U=(Z2*U2-U2*Z2);

for c=1:10;

[p1,F(:,c)]=linsolve((M-h*Z1(c,1)),u);

totbolt=totbolt+exp(-(B*(Z2(c,c)-Z2(1,1))/(temp*kb)));
totbolt1=totbolt1+exp(-(B*(Z2(c,c)-Z2(1,1))/(temp1*kb)));

end

F1=F'*R*F;
F2=F'*S*F;

if hi<1;

else

for cc=1:3;

wd(cc,1)=((wx(cc,1)*J(3,1))^2+(wy(cc,1)*J(3,2))^2+(wz(cc,1)*J(3,3))^2)^0.5;

c=2*(cc-1)+1;

bolt=exp(-(B/(2.0837e10*P)*(Z2(c,c)-Z2(1,1)))/temp)/totbolt;
bolt1=exp(-(B*(Z2(c,c)-Z2(1,1))/(temp1*kb)))/totbolt1;

for d=c+1;

if abs(U(d,c)-P*f/B)<HG/2*(P*f)/(B*H);

V(d,c)=2*H-(U(d,c))*((B*H)/(P*f));
V1(d,c)=2*H-(U1(d,c))*((B*H)/(P*f));

wd1(cc,1)=abs((V(d,c)-V1(d,c))/(U(d,c)-U1(d,c)));

T(:,cc)=T(:,cc)+bolt*((abs(F1(c,d)))^2+(abs(F2(c,d)))^2)*exp(-(((V(d,c)*I-
G)/(wd(cc,1)))^2))/wd(cc,1)*wd1(cc,1);
Q(:,cc)=Q(:,cc)+bolt1*((abs(F1(c,d)))^2+(abs(F2(c,d)))^2)*exp(-(((V(d,c)*I-
G)/(wd(cc,1)))^2))/wd(cc,1)*wd1(cc,1);

else

end

end
```

```
end
end

U1=U;

end

end

end

// Boltzmann distribution

TT=sum(T,'c');
QQ=sum(Q,'c');

scf(20)

delete("all")

subplot(2,1,1)

plot(G,T(:,1),'g')
plot(G,T(:,2),'y')
plot(G,T(:,3),'b')
plot(G,TT,'r')

subplot(2,1,2)

plot(G,Q(:,1),'g')
plot(G,Q(:,2),'y')
plot(G,Q(:,3),'b')
plot(G,QQ,'r')

endfunction
```

S9: Orientation Dependence of the Exchange/Fine Structure tensors

The apparent re-orientation of the exchange and zero-field tensors seen in the simulation of the g~1.9 signal is explored in more detail below. Here all unique orientations of the zero-field tensor (D = 15, E/D = 0.27) relative to the exchange tensor were examined. The exchange tensor was assumed to be axial as seen for the g~1.8 signal (J_X = 0.13, J_Y = 0.58, J_Z = 0.58). Simply increasing the zero-field splitting (without rotation of the fine structure tensor relative to the exchange tensor) had little effect on the structure of the semi-quinone iron signal about the g~2 region. In contrast, a large rotation (>60º) in xz plane resulted in the characteristic splitting of the central peak about g~1.8, now resolving two maxima at g~1.9 and g~1.7. Rotation of the fine structure tensor in the xy plane did not yield a semi-quinone iron signal similar to either the g~1.81 or g~1.9. Rotation in the yz plane is invariant as the exchange tensor is axial; all b angles yield a simulation similar to Fig s9.1 tile 1.

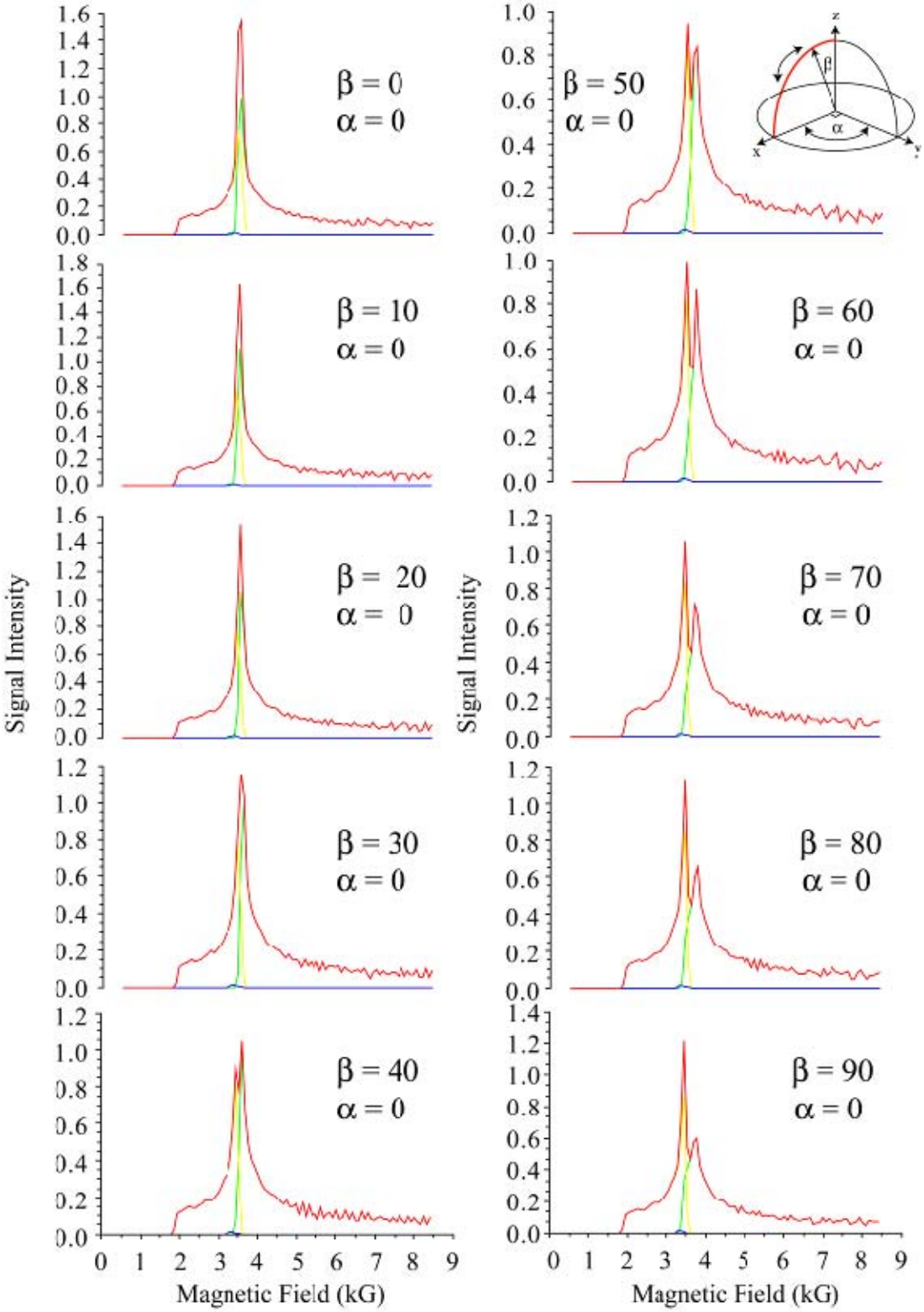
β = 0
α = 0
β = 10
α = 0
β = 20
α = 0
β = 30
α = 0
β = 40
α = 0
β = 50
α = 0
β = 60
α = 0
β = 70
α = 0
β = 80
α = 0
β = 90
α = 0
Signal Intensity
Signal Intensity
Magnetic Field (kG)
Magnetic Field (kG)

Figure s9.1: Tensor orientation dependence of the semi-quinone iron signal assuming a zero-field tensor (D = 15, E/D = 0.27) and axial exchange tensor (J_X = 0.13, J_Y = 0.58, J_Z = 0.58) in the xz plane. The orientation of the zero-field tensor relative to the exchange tensor is given in the corner of each individual tile.

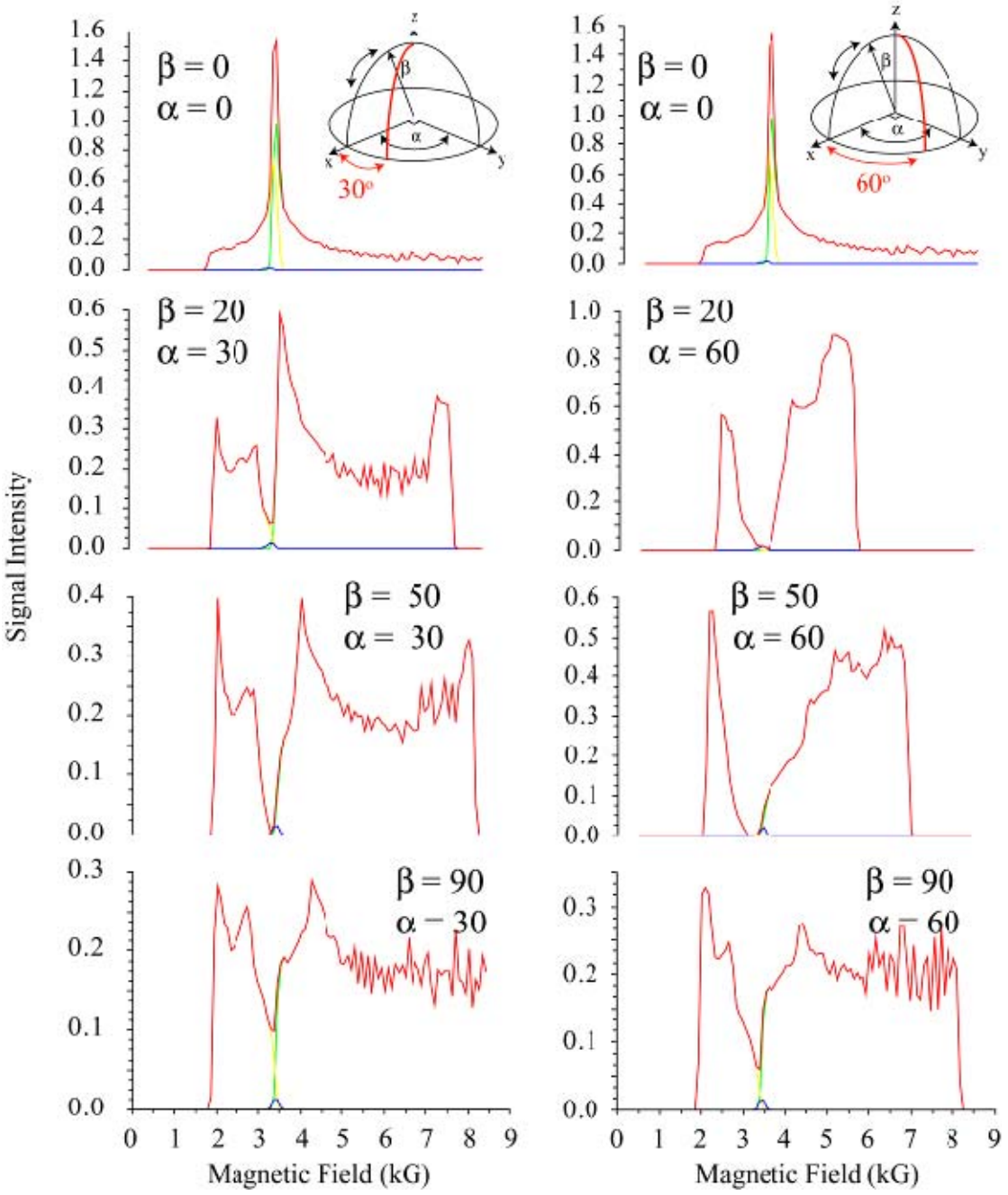

Figure s9.2: Tensor orientation dependence of the semi-quinone iron signal assuming a zero-field tensor (D = 15, E/D = 0.27) and axial exchange tensor (J_X = 0.13, J_Y = 0.58, J_Z = 0.58) in the xyz quadrant. The orientation of the zero-field tensor relative to the exchange tensor is given in the corner of each individual tile.

The orientation of the zero-field tensor for the 5 quinone-iron complexes as calculated by DFT follows a similar trend to that seen for the hyperfine tensor of the iron, as shown in Fig. 7. For both BRC and PS II where the 5^{th} ligand is glutamate, formate or bicarbonate, the largest tensor component (in absolute magnitude and assigned to D_Z), is directed towards Q_A^-. For BRC (+ glutamate or formate), the D_Y direction bisects the 5^{th} ligand, whereas the D_X is directed towards the axial histidine, defining a plane characterized by lower tensor values (in absolute magnitude). As seen for the hyperfine tensor, the orientation of the zero-field tensor does not dramatically change between BRC and PS II. In PS II (+ formate or bicarbonate), the D_X/D_Y plane still contains axial histidines and the 5^{th} ligand but now D_X points to the axial histidine and D_Y is directed towards one of the binding oxygens rather than carbon of the carboxyl group. In contrast, for PSII (+ carbonate), D_Z is now the smallest tensor component (in absolute magnitude) and is rotated into the membrane plane, pointing towards one of the axial histidines. The D_X/D_Y plane still contains 5^{th} ligand (CO_3^{2-}) but it now also contains the equatorial histidines with D_X and D_Y components directed towards the binding nitrogens of the histidines. As with the analysis of the hyperfine tensor above, the apparent *interchange* of the principal values of the zero-field tensor for PS II (+ carbonate) as compared to all other model systems is qualitatively similar to the change inferred from the ESR simulations discussed above. Here it was shown that the exchange tensor re-orientates relative to the fine-structure tensor for the simulation g~1.9 signal as compared to the simulation g~1.81 signal.

S10: Orientation dependence of the g~1.9 signal

The orientation dependence of the g~1.84 and g~1.9 semiquinone-iron signals has been previously determined (*11*). It was shown that the turning point of the semiquinone-iron signal (for either g~1.84 or g~1.9) was maximal normal to the membrane plane. The present analysis (and the analysis of Butler et al 1984) is compatible with these data.

The orientation dependence of g-values is distributed over a relatively large field space in the xy or yz planes. Only in the xz plane is the simulated spectrum narrow. These features dominate the derivative EPR signal and are resolved in orientation studies (see Fig. s10).

This result allows the assignment of the y axis (as yet arbitrarily defined) of the system. It must be in a direction *parallel* to the membrane plane. The coupling change (that occurs upon inter-conversion of the g~1.84 to g~1.9 signals) must then involve a change in the coupling environment generally within a plane perpendicular to the membrane. This is consistent with the inferred coupling change between the g~1.84 and g~1.9 forms as determined by DFT.

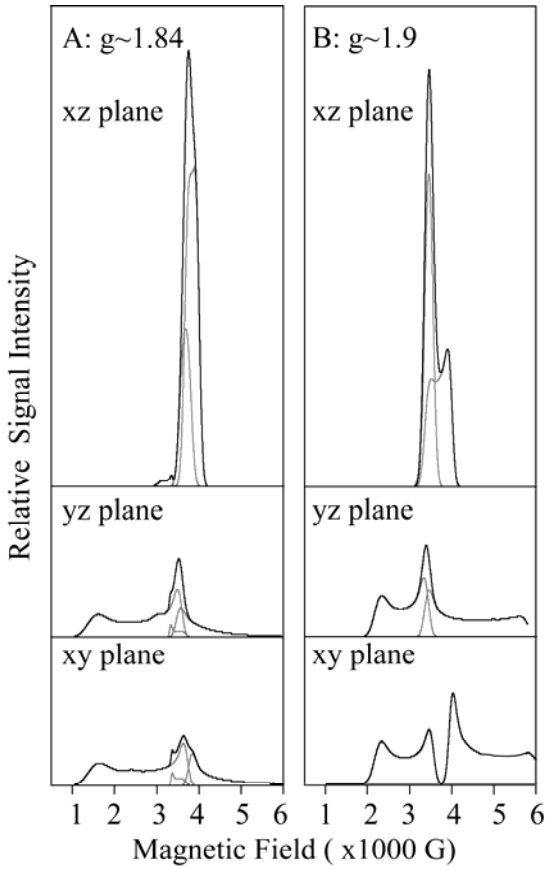

Figure s10: The orientation dependence of the simulated g~1.84 (A) and g~1.9 (B) ESR absorbance signals. Calculated spectra represent the two dimensional powder pattern for the either semi-quinone iron signals in the xz, yz and xy planes.

Supporting Information reference list

1. Butler, W.F., R. Calvo, D.R. Fredkin, R.A. Isaacson, M.Y. Okamura, and G. Feher. 1984. The electronic structure of Fe2+ in reaction centres from *Rhodopseudomonas sphaeroides*. III. EPR measurements of the reduced acceptor complex. *Biophys. J.* 45:947-973.
2. Butler, W.F., R. Calvo, D.R. Fredkin, R.A. Isaacson, M.Y. Okamura, and G. Feher. 1980. The electronic structure of Fe2+ in reaction centers from *Rhodopseudomonas sphaeroides* I. Static magnetization measurements. *Biophys. J.* 45:947-973.
3. Allen, J.P., G. Feher, T.O. Yeates, H. Komiya, and D.C. Rees. 1988. Structure of the Reaction Center from *Rhodobacter sphaeroides* R-26: Protein-Cofactor (Quinones and Fe2+) Interactions. *Proc. Natl. Acad. Sci. USA* 85(22):8487-8491.
4. Deisenhofer, J., O. Epp, K. Miki, R. Huber, and H. Michel. 1985. Structure of the protein subunits in the photosynthetic reaction centre of *Rhodopseudomonas viridis* at 3 Å resolution. *Nature* 318(6047):618-624.
5. Ferreira, K.N., T.M. Iverson, K. Maghlaoui, J. Barber, and S. Iwata. 2004. Architecture of the Photosynthetic Oxygen-Evolving Center. *Science* 303:1831-1838.
6. Loll, B., J. Kern, W. Saenger, A. Zouni, and J. Biesiadka. 2005. Towards Complete Cofactor Arrangement in the 3.0 Å Resolution Crystal Structure of Photosystem II. *Nature* 438:1040-1044.

7. Abragram, A., and B. Bleaney. 1970. Electron Paramagnetic Resonance of Transition Metal Ions. Clarendon Press, Oxford.
8. Rose, M.E. 1967. Elementary theory of angular momentum. Goeppert MM, editor. John Wiley & Sons Inc, Sydney.
9. Carrington, A., and A.D. McLachlan. 1967. Introduction to Magnetic Resonance. Rice SA, editor. Harper and Row, New York.
10. Aasa, R., and T. Vanngard. 1975. EPR signal intensity and powder shapes: A reexamination. *J. Magn. Reson.* 19(3):308-315.
11. Rutherford, A.W. 1985. Orientation of EPR signals arising from components in Photosystem II membranes. *Biochim. Biophys. Acta* 807(2):189-201.